



HAL
open science

Molecular dynamics simulation of the interaction of uranium (VI) with the C–S–H phase of cement in the presence of gluconate

Iuliia Androniuk, Andrey G. Kalinichev

► To cite this version:

Iuliia Androniuk, Andrey G. Kalinichev. Molecular dynamics simulation of the interaction of uranium (VI) with the C–S–H phase of cement in the presence of gluconate. *Appl.Geochem.*, 2020, 113, pp.104496. 10.1016/j.apgeochem.2019.104496 . hal-02510532

HAL Id: hal-02510532

<https://hal.science/hal-02510532>

Submitted on 15 Feb 2022

HAL is a multi-disciplinary open access archive for the deposit and dissemination of scientific research documents, whether they are published or not. The documents may come from teaching and research institutions in France or abroad, or from public or private research centers.

L'archive ouverte pluridisciplinaire **HAL**, est destinée au dépôt et à la diffusion de documents scientifiques de niveau recherche, publiés ou non, émanant des établissements d'enseignement et de recherche français ou étrangers, des laboratoires publics ou privés.

1 Molecular Dynamics Simulation of the Interaction of Uranium (VI)
2 with the C-S-H Phase of Cement in the Presence of Gluconate

3
4
5 Iuliia Androniuk^{1,*}, Andrey G. Kalinichev^{1,2}

6 ¹ Laboratoire SUBATECH (UMR 6457 – Institut Mines-Télécom Atlantique,
7 Université de Nantes, CNRS/IN2P3), 44307, Nantes, France

8 ² National Research University Higher School of Economics, Russian Federation

9
10
11
12
13
14 * Corresponding author: E-mail address: yuliya.andronyuk@gmail.com

15

1 **Abstract**

2 Due to their high durability and immobilization properties, cementitious materials
3 have found a considerable application in the design and construction of radioactive
4 waste repositories in the last decades. During cement paste production, organic
5 additives are introduced to modify various properties of cement. The presence of such
6 organic complexants may negatively affect the immobilizing properties of cement with
7 respect to radionuclides. For better understanding and prediction of the effects of
8 interactions between organic molecules and cementitious materials with radionuclides,
9 we have developed several representative models consisting of three principal
10 components: (i) calcium silicate hydrate (C-S-H) phase - the main binding phase of
11 cement; (ii) gluconate, a simple well-described molecule, as a representative of organic
12 additives; (iii) U(VI), as one of the most studied radionuclides of the actinide series. The
13 C-S-H phase with low Ca/Si ratio (~0.83) typical for “low-pH” and degraded cement
14 pastes has been selected for this modelling study. Structural, and energetic aspects of
15 the sorption processes of uranyl, gluconate, and their mutual correlations on the surface
16 of cement were quantitatively modeled by classical molecular dynamics (MD) and
17 potential of mean force (PMF) calculations. The ternary surface complex formation
18 between uranyl hydroxides and Ca^{2+} cations at the C-S-H aqueous interfaces is shown
19 to have an important role in the overall sorption process. In the presence of gluconate,
20 U(VI) sorption on C-S-H is facilitated by weakening the Ca^{2+} binding with the surface.
21 Additionally, Na^+ is proven to be an important competitor for certain surface sorption
22 sites and can potentially affect the equilibrium properties of the interface.

23 **Key words** C-S-H, cement, uranyl, gluconate, sorption, molecular dynamics simulation

1 **1. Introduction**

2 Cementitious materials are widely used in the design and construction of
3 geological radioactive waste repositories, in particular in the Callovo-Oxfordian
4 argillaceous rock formation in the East of the Parisian basin in France (e.g., Grambow,
5 2016; Kořátková et al., 2017). They are the principal construction material for the waste
6 storage galleries and access shafts of the underground repositories, but can also serve
7 as part of the packaging for some intermediate level waste or as the sealing material for
8 storage cells.

9 Calcium silicate hydrate (C-S-H) is the main binding phase of cements and controls
10 their mechanical and chemical durability. C-S-H phases are formed as a result of
11 hydration of alite (Ca_3SiO_5) and industrial belite (Ca_2SiO_4), the two silicates that are the
12 essential constituents of cement clinker (Taylor, 1997; Richardson, 2010). Because of its
13 critical role, C-S-H was selected as the cement model in this work. However, an
14 accurate nano-scale description of C-S-H phases is very challenging and the interest in
15 understanding their atomistic structure and the nature of structural disorders continues
16 to be strong. A significant amount of research has been devoted recently to clarify these
17 issues using various experimental and theoretical approaches, and there is now a
18 general consensus that the C-S-H phases have structural similarity with such minerals
19 as tobermorite and jennite (Cong and Kirkpatrick, 1996; Yu et al., 1999; Pellenq et al.,
20 2009; Richardson et al., 2010; Grangeon et al., 2016, 2017; Kumar et al., 2017). It is
21 also established that Ca/Si ratio is a single most important characteristic of the C-S-H
22 phase which significantly affects such chemical and physical properties of cement as pH

1 of the pore water, the surface charge, and equilibrium ion concentrations (Chen et al.,
2 2004; Lothenbach and Nonat, 2015).

3 The atomistic models of C-S-H used in this study to simulate the interaction of
4 actinides with cement in the context of radioactive waste repository environment were
5 constructed on the basis of experimental observations and earlier computer simulations.
6 They provide a compromise between the necessity to realistically represent the true
7 compositional and structural complexity of the C-S-H phase and still maintain relative
8 simplicity, which should facilitate better quantitative investigation of the specific
9 molecular mechanisms of interaction among different chemical species near the surface
10 (Androniuk et al., 2017).

11 The sorption behavior of actinides on C-S-H phases has already been studied
12 recently, and a strong effect of the Ca/Si ratio has been found (Pointeau et al., 2004;
13 Harfouche et al., 2006; Tits et al., 2011; Gaona et al., 2012; Macé et al., 2013; Häußler
14 et al., 2018; Tits and Wieland, 2018). Even though in ordinary Portland cement we can
15 observe predominantly C-S-H phases with Ca/Si ratios higher than 1.5, lower ratios are
16 typical for “low-pH” cements with added fly ash and silica fume, and in degraded cement
17 pastes because of the decalcification (Glasser et al., 2008). As the first step, C-S-H
18 phases with low Ca/Si ratio (~ 0.83) have been selected for this modelling study.

19 During cement paste production, various kinds of organic additives are typically
20 used to enhance mechanical properties of the final cement material, and the presence of
21 these potentially reactive and mobile chemicals may cause additional safety concerns
22 (Keith-Roach, 2008). Consequently, the molecular mechanisms of their interaction with

1 all components of the waste storage system should be systematically studied,
2 quantitatively described, and understood in detail. Several recent studies shed light
3 upon the behavior of organics in cementitious materials (Nalet and Nonat, 2016;
4 Chaudhari et al., 2017; Orozco et al., 2017) and their effect on the mobility of
5 radionuclides in cement (Pointeau et al., 2006, 2008; García et al., 2018). However, to
6 our knowledge, the molecular mechanisms controlling the behavior of the ternary
7 systems (C-S-H/radionuclide/organic) have not yet been investigated. In the present
8 work, we are addressing this gap by atomistic computer simulations of a model ternary
9 system. Gluconate ($C_6H_{12}O_7$) ion, a relatively simple hydroxy acid that is chemically
10 stable in alkaline solutions, is used here as a proxy model for organic additives, while
11 U(VI), one of the most important and well-studied actinide elements, is used as a model
12 radionuclide.

13 The structural defects in the C-S-H surface silicate chains can serve as potential
14 sorption sites for the interfacial species. The variations in structure and surface charge
15 distribution of the C-S-H surface models create different opportunities for the cations to
16 bind. However, not all of the binding sites are equivalent, some of them offer more
17 favorable local steric environments and/or lower energies for stronger binding. This is
18 where the computational molecular modelling becomes very helpful by providing a
19 detailed quantitative atomic scale picture of the site-specific interactions on the interface.
20 A combinational analysis of the local structures, density profiles and surface maps for
21 target atoms gives an insight of what are the preferential sorption sites on the C-S-H
22 surface (Androniuk et al., 2017).

1 A number of studies (Viallis-Terrisse et al., 2001; Hill et al., 2006; Sugiyama, 2008;
2 Labbez et al., 2011; Bach et al., 2013; Henocq, 2017; Dufresne et al., 2018) have
3 demonstrated that the presence of alkali on the interface of C-S-H can significantly
4 change its equilibrium solution and surface physical and chemical properties: they can
5 affect the surface zeta potential, compete for the sorption sites. Taking this into account
6 consideration, Na⁺ is introduced to the simulated systems as a counter ion of gluconate.
7 The free energies of adsorption for the ions of interest (Ca²⁺, UO₂²⁺, gluconate, Na⁺) at
8 different surface sites of calcium silicate hydrates are calculated, analyzed, and
9 discussed in this paper.

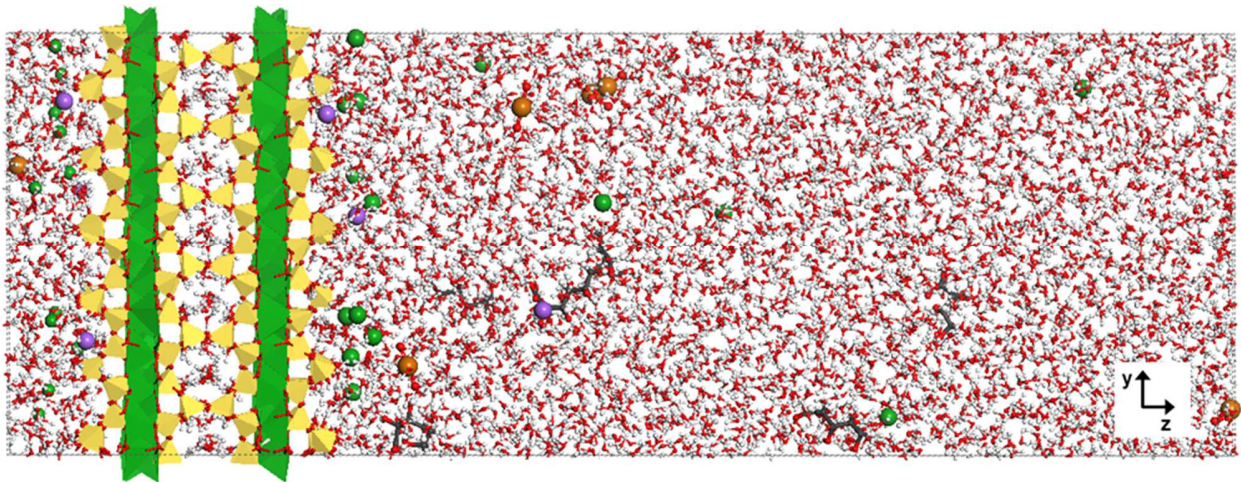
10

11 **2. Methods**

12 The atomistic model of the C-S-H surface for our simulations was constructed
13 based on the crystal structure of tobermorite, that was proven to be the closest to the
14 real cement hydrate (e.g., Grangeon et al., 2016, 2017; Kumar et al., 2017; Kunhi
15 Mohamed et al., 2018). First, the tobermorite crystallographic unit cell
16 (Ca₅Si₆O₁₆(OH)₂·4H₂O; Hamid, 1981; Merlino et al., 2001) has been multiplied along the
17 *a* and *b* directions (6 × 6 × 1) to create the crystal supercell of the dimensions
18 40.2 × 44.4 × 25.5 Å³. This supercell was then cleaved in the middle of interlayer along
19 the (0 0 1) crystallographic plane to create a basic model of the C-S-H surface. Next, the
20 top layers of the cleaved crystal were modified by randomly removing the bridging Si
21 tetrahedra in accordance with available experimental NMR and IR data (Cong and
22 Kirkpatrick, 1996; et al., 1999; Beaudoin et al., 2009; Roosz et al., 2018), and
23 introducing additional Ca²⁺ cations into the interlayer (Fig. 1). The protonation state of

1 surface silanol groups was assigned based on the theoretical considerations (Churakov
2 et al., 2014), and adjusted to correspond the range of pH ~ 10-11 typical of C-S-H with a
3 low Ca/Si ratio. More specifically, all silanol groups of bridging Si and one of the pairing
4 Si (replacing the introduced defect) were deprotonated. The deprotonated oxygens of
5 the surface were assigned a partial charge of $q_{\text{onb}} = -1.3|e|$, higher than the protonated
6 ones in the standard ClayFF model (see Kirkpatrick et al., 2005a, 2005b, and the
7 discussion below). The structural defects were not introduced for the silicate chains
8 inside the bulk tobermorite substrate, since only the surface interactions are the principal
9 focus of the present work.

10



11
12 **Figure 1.** A snapshot of the entire simulation supercell. The color scheme is as follows:
13 Si – yellow; Ca – green; O – red; H – white; Na – violet; U – dark-orange; and
14 C – dark-grey.

15

1 The interfacial aqueous solution contained 6 ions of Na^+ , $\text{UO}_2(\text{OH})^{3-}$, and gluconate
2 each, with ~ 4500 H_2O molecules, that approximately corresponds to 0.07 M ion
3 concentrations. These relatively high concentrations had to be used in the simulations
4 for better statistical sampling of the model systems, but they should not affect overall
5 results. Three dimensional periodic boundary conditions (Allen and Tildesley, 2017)
6 were applied to the constructed model interfaces, and the thickness of the solution layer
7 between the two C-S-H surfaces was large enough (≈ 70 Å) to ensure that the
8 interactions at one surface would not affect the other, and result in bulk-like solution
9 behavior in the middle of the model simulation box (Fig. 1).

10 The interatomic interaction parameters for C-S-H, H_2O , and Ca^{2+} ions were taken
11 from the ClayFF parameterization (Cygan et al., 2004), and its later modifications for
12 cement systems (Kirkpatrick et al., 2005b; Kalinichev et al., 2007; Mishra et al., 2017).
13 Polarizability of actinides, such as U(VI), can generally be considered as an important
14 factor contributing to overall interatomic interactions (Clavaguera-Sarrio et al., 2003;
15 Newcomb, 2018; Duvail et. al., 2019). However, in our simulations U(VI) is only present
16 in the form of a uranyl cation, UO_2^{2+} , and non-polarizable force field parameterization for
17 such species has long been already proven to be a good compromise providing
18 accurate simulation results validated by experimental data (Guilbaud and Wipff, 1996;
19 Greathouse et al., 2002; Kerisit and Liu, 2014). The interaction parameters for uranyl
20 ions used in this work (Guilbaud and Wipff, 1996) are also consistent with ClayFF
21 (Teich-McGoldrick et al., 2014).

22 Based on the recent comparison of several clay-organic force field combinations
23 (Szczerba and Kalinichev, 2016), the general AMBER force field GAFF (Wang et al.,

1 2004) was used to describe the interatomic interactions involving gluconate ions.
2 Standard Lorentz-Berthelot mixing rules (Allen and Tildesley, 2017) were applied to
3 calculate short-range Lennard-Jones interactions between the unlike atoms (with a cut-
4 off distance of 14 Å). Long-range electrostatic forces were evaluated by means of the
5 Ewald summation method. All molecular dynamics (MD) simulations were performed
6 using LAMMPS software package (Plimpton, 1995). The Newtonian equations of atomic
7 motions were numerically integrated with a timestep of 1 fs, and the model systems
8 were initially equilibrated for 3 ns in the isobaric–isothermal statistical ensemble (*NPT*),
9 then for 2 ns in the canonical ensemble (*NVT*). Temperature and pressure were
10 constrained using the Nose-Hoover thermostat and barostat (Allen and Tildesley, 2017)
11 at ambient conditions ($T = 300$ K, $P = 0.1$ MPa). Model equilibration was carefully
12 monitored by assessing the temperature, pressure, kinetic and potential energy of the
13 system, and dimensions of the simulation box, in order to confirm that these parameters
14 reach their equilibrium steady state values on average (Braun et al., 2019).

15 To probe the structure of bulk aqueous solutions for comparison with the interfacial
16 solutions, several preliminary MD simulation runs were performed for the systems
17 containing pairs of ions ($\text{UO}_2(\text{OH})_3^-$, Ca^{2+} , $\text{Ca}(\text{OH})^+$, Na^+ , and gluconate) placed in a
18 cubic $40 \times 40 \times 40$ Å³ simulation box filled with H₂O molecules at a density
19 corresponding to ambient conditions. When necessary, aqueous OH⁻ and Na⁺ ions were
20 added to maintain the total electrostatic neutrality of the models.

21 In the first series of unconstrained MD simulations, the most probable sorption
22 sites on the C-S-H surfaces were determined based of the calculation of time-averaged
23 atomic density profiles in the direction perpendicular to the surface, and atomic density

1 distributions parallel to the surface in the layer of solution nearest to it. The local atomic
2 density is calculated through the evaluation of the average number of atoms of a certain
3 type (\bar{N}_A) found at a distance z (i.e, within the range of distances from z to $z+\Delta z$) parallel
4 to the surface:

$$5 \quad \text{Density}_A = \frac{\bar{N}_A (\Delta z)}{V_{cell}}$$

6 where V_{cell} is the total volume of the simulation cell, $\Delta z = 0.1 \text{ \AA}$. The two-dimensional
7 distributions in the xy plane within a layer of solution parallel to the surface at a certain
8 distance z are defined by the probability of finding an atom of type A at a position (x,y)
9 above the surface within a range of distances from z to $(z+\Delta z)$:

$$10 \quad \text{Surface density}_A(x,y) = \bar{N}_A(\Delta x \Delta y)$$

11 where $\Delta z = 2 \text{ to } 5 \text{ \AA}$, $\Delta x = \Delta y = 0.2 \text{ \AA}$.

12 The change of free energy is the driving force of any process, such as surface
13 sorption. In this case, the difference in free energy between different states of the
14 system (surface-sorbed ion vs the same ion in bulk aqueous solution) along a reaction
15 coordinate can quantitatively characterize the strength of the adsorption sites of interest.
16 Free energy is related to the probability distribution of the thermodynamic states along
17 the reaction coordinate, and statistical analysis of an MD simulation trajectory allows one
18 to quantitatively evaluate free energy evolution in the system using the so-called
19 "umbrella sampling" algorithm or potential of mean force (PMF) calculation (Allen and
20 Tildesley, 2017).

1 A complete calculation requires a number of separate independent simulations to
2 cover the entire range of the reaction coordinate. In each of these "sampling windows"
3 the distance between the reacting species is restrained at a required value using a
4 harmonic force to allow the system to sample all possible configurations around that
5 particular value of the reaction coordinate. The histograms of such simulation series are
6 carefully monitored to ensure adequate and relatively uniform sampling along the
7 reaction coordinate and sufficient overlaps of the sampling windows with each other.
8 This ensures proper recovery of the unbiased PMF curve from the simulated ensemble
9 of the biased histograms using the weighted histogram analysis method (WHAM). A
10 detailed description of the umbrella sampling and WHAM algorithms used here can be
11 found in literature (Kästner, 2011; Grossfield, 2014).

12 Here we additionally used the recently developed approach of site-specific PMF
13 calculations (Loganathan and Kalinichev, 2017) where an additional weak xy constraints
14 were applied as a "soft cylindrical wall" of a small diameter in order to keep the atom
15 above a defined sorption site on the surface and not to allow its significant drift in the
16 directions parallel to the surface. In this way, quantitative description of the adsorption
17 free energy profiles was obtained for UO_2^{2+} , $\text{UO}_2(\text{OH})_3^-$, Ca^{2+} , and Na^+ ions as functions
18 of their distance between each other in bulk aqueous solutions, and from the C-S-H
19 surface at the aqueous interfaces with solutions of various compositions (with and
20 without gluconate present in the system). For each PMF curve obtained, approximately
21 90 constrained MD simulations (sampling windows) were run in the NVT ensemble ($T =$
22 300 K) for 1 ns . Monte Carlo bootstrapping approach implemented in WHAM algorithm
23 has been used to evaluate the statistical uncertainties (Grossfield, 2014; Grossfield et

1 al., 2018). The calculated average value of 0.02 kcal/mol is taken as an estimate of
2 uncertainty for all PMF curves presented in this work.

3

4 **3. Results and Discussion**

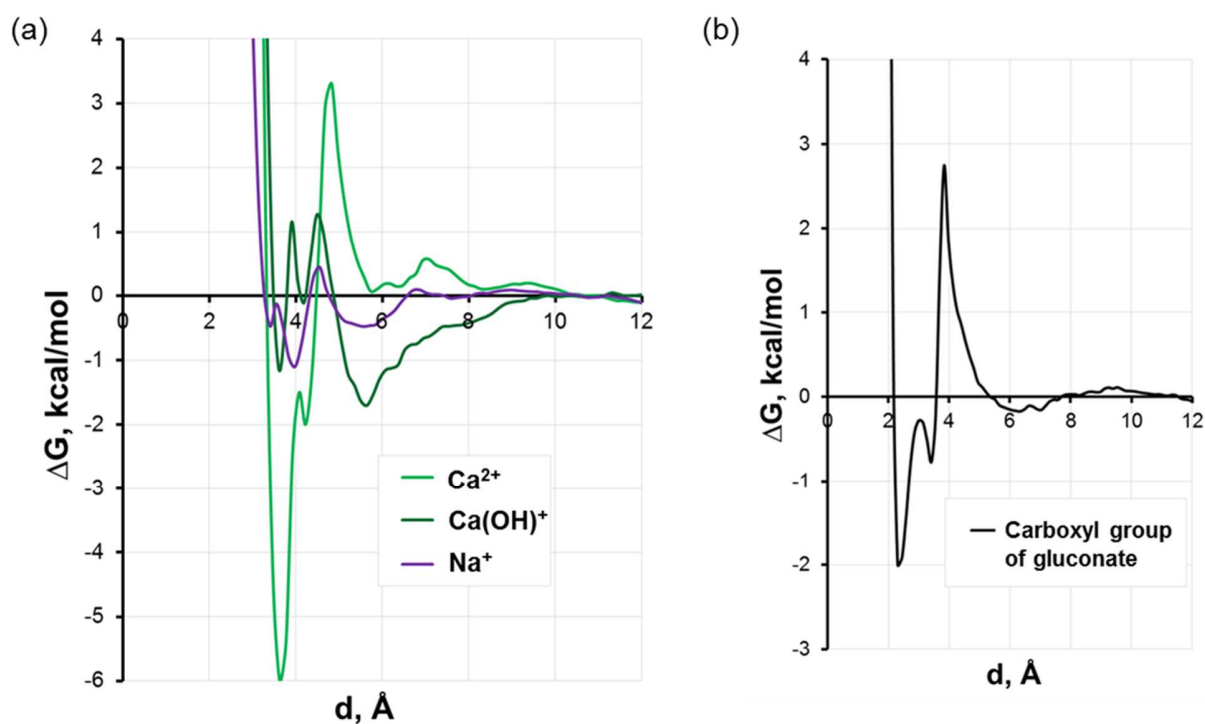
5 **3.1. Complexation of UO_2^{2+} in aqueous solutions**

6 Uranium (VI) exists in aqueous solutions in the form of uranyl cation, UO_2^{2+} , and in
7 alkaline solutions it forms hydroxocomplexes of different stoichiometry with a general
8 formula $(\text{UO}_2)_m(\text{OH})_{n^{2m-n}}$ (Choppin and Mathur, 1991; Krestou and Panias, 2004; García-
9 Hernández et al., 2006; Moll et al., 2014; Drobot et al., 2016). Hydroxyl ions in the
10 coordination sphere of UO_2^{2+} are negatively charged, and different properties are
11 expected for the hydrolysed species compared to the aqua complexes in solutions at
12 lower pH. To better understand the sorption behaviour of $\text{UO}_2(\text{OH})_3^-$ on C-S-H surfaces,
13 a series of PMF calculations were performed for the selected pairs of ions in bulk
14 aqueous solutions (Fig. 2).

15 Formation of calcium uranate carbonate complexes is known for carbonated
16 systems (Dong et al., 2005; Fox et al., 2006; Stewart et al., 2010; Smith et al., 2015;
17 Richter et al., 2016; Saleh et al., 2018), but in the absence of CO_2 a formation of
18 hydroxo complexes can be suggested where cations are bound with a hydroxyl “bridge”.
19 The stabilisation by Ca^{2+} in alkaline solutions has been already proven for a number of
20 actinides (Altmaier et al., 2008; Rabung et al., 2008; Fellhauer et al., 2010, 2016) and
21 thus is also expected for U(VI). From the PMF profiles in Fig. 2(a) it can be clearly seen
22 that there is a strong interaction between aqueous $\text{UO}_2(\text{OH})_3^-$ and Ca^{2+} ions: a stable

1 complex is formed with the energy barrier about 10 kcal/mol. Two main energy minima
2 found at interionic distances of ~ 4.1 and ~ 3.6 Å correspond to the formation of one and
3 two OH⁻ bridges, respectively.

4



5

6 **Figure 2.** The potential of mean force as a function of distance between $\text{UO}_2(\text{OH})_3^-$ and
7 cations (a) or carboxyl group of gluconate (b) in aqueous solution.

8

9 A fraction of calcium in alkaline solution can be present as $\text{Ca}(\text{OH})^+$, and a free
10 energy profile for this pair has also been calculated. The energy minima are found at the
11 same distance as for Ca^{2+} cation but the formed complexes have much lower stability:
12 the energy barriers are about 2.2 kcal/mol at ~ 3.6 Å and 1.7 kcal/mol at 5.5 Å.

1 Additionally, Na^+ has been studied as a potentially competitive cation that is introduced
2 into the system as a counterion of gluconate, and it is one of the major cations present in
3 the real cement pore water. Sodium only weakly interacts with uranyl hydroxide in water
4 showing only two shallow minima at distances of ~ 3.3 and ~ 4.0 Å. As it can be seen, the
5 double free energy minimum is found for all the ions studied. The complexation of U(VI)
6 with $\text{Ca}(\text{OH})^+$ and Na^+ can be considered weak, and these interactions should not
7 interfere significantly with its uptake by C-S-H.

8 Uranyl can form complexes with more than one gluconate anion under alkaline
9 conditions (Birjkumar et al., 2011; Colàs et al., 2013). The cation will mostly coordinate
10 with deprotonated carboxyl groups of organic ion, but at highly alkaline solutions
11 ($\text{pH} > 13.9$) the gluconate hydroxyl groups can be deprotonated and can also participate
12 in U(VI) complexation. The plot in Fig. 2(b) shows the free energy of binding a gluconate
13 carboxyl group to the $\text{UO}_2(\text{OH})_3^-$ ion. Even though both ions are negatively charged,
14 complexation is possible due to the presence of an exchangeable water molecule in the
15 solvation shell of $\text{UO}_2(\text{OH})_3^-$. The calculation results show that the energy required to
16 replace this water molecule by gluconate is ~ 5 kcal/mol. The distinct energy minima
17 found at ~ 2.5 Å ~ 3.4 Å corresponding to the direct binding of U(VI) to the oxygens of the
18 carboxyl group. The difference in the distance between the two of them can be
19 explained by the different binding configuration of the organic molecule. In addition, it
20 was observed that these complexes are stabilised by formation of hydrogen bonds
21 between the oxygen of aqueous OH^- ion and one or two hydrogens of the closest
22 gluconate alcohol functional groups.

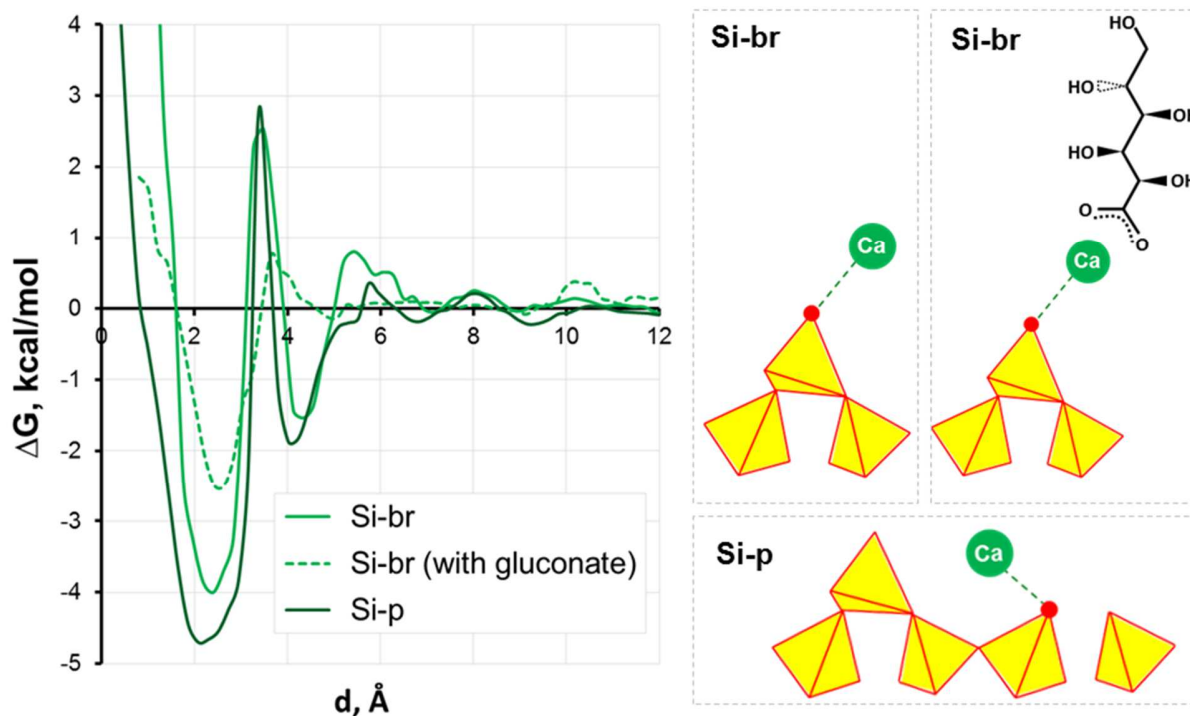
1 To summarize, the combination of the results for U(VI) in solution with the available
2 literature data allows us to suggest that complex formation between uranyl hydroxides
3 and Ca^{2+} cations present at aqueous C-S-H interfaces should play a significant role in
4 the sorption process. Meanwhile, complexation with other interfacial ions is minor, but
5 cannot be excluded completely.

6 **3.2. Complexation of Ca^{2+} and Ca-gluconate at the C-S-H interface**

7 The deprotonated silanol groups can be considered the most reactive groups of the
8 C-S-H surface due to their high negative charge. Two typical sorption sites for Ca^{2+} on
9 the C-S-H surface were selected for the PMF calculations in order to obtain quantitative
10 information on the site-specific adsorption free energy: the deprotonated silanol group of
11 the bridging silicon tetrahedron, and the deprotonated silanol group of the pairing silicon
12 tetrahedron (the schematic representations of the sites are shown in Fig. 3).

13 The adsorption free energy profiles calculated for Ca^{2+} cations above two selected
14 binding sites in Fig. 3 with and without gluconate demonstrate that in the absence of
15 organics the energy of adsorption is nearly the same for both sorption sites sampled.
16 The first energy minimum (at $d \approx 2.5 \text{ \AA}$) corresponds to the inner-sphere coordination to
17 the deprotonated surface oxygen, while the second pronounced minimum (at $d \approx 4.2 \text{ \AA}$)
18 – to the outer-sphere coordination. The energy barrier between the inner- and outer-
19 sphere complexes is 7.5 kcal/mol for the bridging Si site and 6.5 kcal/mol for the pairing
20 Si site. This means that the complexation of Ca^{2+} with C-S-H surface is strong and a
21 relatively high energy is required to replace the bound cation by another ion or molecule
22 on the site.

1



2

3 **Figure 3.** Adsorption free energy profiles as functions of the distance between Ca^{2+} ion
4 and the deprotonated silanol groups on the C-S-H surface. The schematic
5 representation of the two distinct sorption sites (Si-br – bridging Si
6 tetrahedron; Si-p – pairing Si tetrahedron) is shown on the right.

7

8 It is important to note that Ca^{2+} cations are not located strictly above the selected
9 sorption sites, so the position of the first minimum does not represent the binding
10 distance, but shows only how close the cation is to the surface on average; the z-
11 coordinate of the deprotonated oxygen is taken as a reference of zero distance.

1 In our study, we consider that the cement system was equilibrated with organics
2 prior to contact with U(VI). The C-S-H phases with low Ca/Si ratio would typically have a
3 high number of bridging sites, therefore, these sites were selected to study the sorption
4 of a Ca^{2+} gluconate complex in the PMF calculation, where constraints were applied only
5 to the Ca^{2+} ion. At high pH, the formation of very stable multinuclear Ca-gluconate
6 complexes is expected (Pallagi et al., 2014). Nevertheless, the concentrations of
7 gluconate used here are far too low to observe such complexation. In the absence of
8 ligand excess, cation complexation with deprotonated carboxyl group is the most
9 probable interaction that is mostly driven by electrostatic forces.

10 The free energy of adsorption (dashed green line in Fig. 3) is noticeably different
11 for Ca^{2+} when a carboxyl group of the gluconate contributes to the first coordination
12 sphere of the cation. The first minimum at $d \approx 2.5 \text{ \AA}$ is due to the same inner-sphere
13 complexation as for the organic-free system, but the energy necessary to replace
14 surface oxygen by a water molecule is lower by half in the presence of gluconate,
15 $\sim 2.5 \text{ kcal/mol}$. Also, the second energy minimum corresponding to the outer-sphere
16 complexation disappears. Accordingly, the binding of Ca^{2+} to the C-S-H surface
17 becomes much weaker and potentially may result in a higher probability of substitution
18 for a competing solution cation (e.g., Na^+ or UO_2^{2+}).

19 **3.3. Complexation of UO_2^{2+} , $\text{UO}_2(\text{OH})_3^-$, and Na^+ on the C-S-H surface**

20 The MD simulations of UO_2^{2+} cations without ligands at the C-S-H surface have
21 been performed here in order to understand the effects of aqueous hydroxyl ions and
22 dissolved organics on the surface adsorption. UO_2^{2+} cations are bound to the same

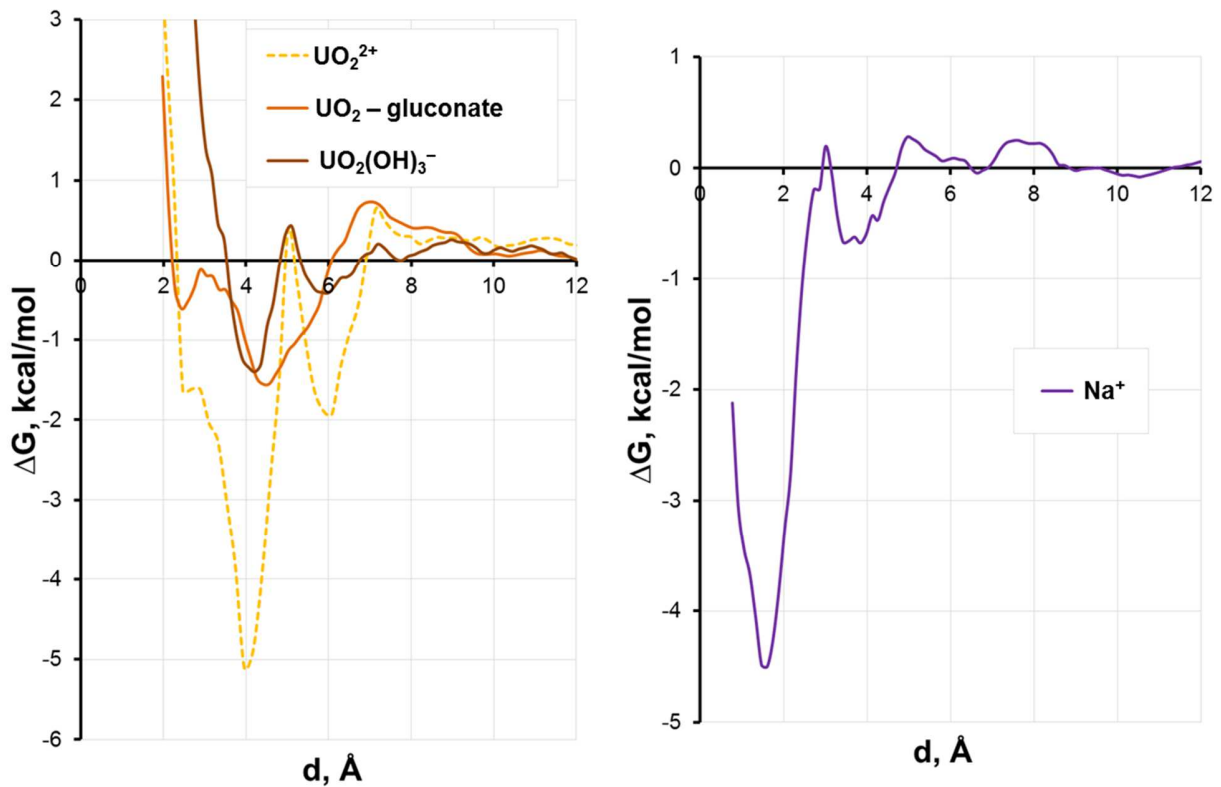
1 surface sites as Ca^{2+} cations and a competition between them can be expected as it
2 was previously discussed (Androniuk et al., 2017). A preferential UO_2^{2+} sorption on the
3 deprotonated sites is observed. The adsorption free energy profile of the uranyl cation
4 as a function of distance from the Si-bridging site is presented in Fig. 4 (dashed line).
5 There are two main energy minima at ~ 4.0 and ~ 6.0 Å from the surface which
6 correspond to the formation of the inner- and outer-sphere surface complexes,
7 respectively. Compared to Ca^{2+} , UO_2^{2+} binds farther from the surface and the energy
8 barrier for the transition between two surface complexes is about 5.5 kcal/mol, which is
9 2 kcal/mol lower. UO_2^{2+} will preferably bind with the deprotonated oxygen as an inner-
10 sphere complex on the Ca-free sites or on the sites where Ca^{2+} is sorbed as an outer-
11 sphere complex, since the energy necessary to substitute the directly bound Ca^{2+} cation
12 is relatively high.

13 The PMF oscillations seen in Fig. 4 can be associated with the local structural
14 properties of the interface for the selected cation and sorption site: the influence of other
15 neighboring ions, the high negative charge of the surface, and the H_2O surface
16 rearrangements through hydrogen bonding, etc.

17 The general trends of $\text{UO}_2(\text{OH})_3^-$ sorption behaviour have been first analysed from
18 the unconstrained MD simulations. The atomic density profiles (Fig. 5(a)) show that the
19 closest peak for U(VI) is found at a distance of $\sim 4\text{-}5$ Å from the position of the top-most
20 surface silanol groups. The direct binding has not been observed during the
21 unconstrained simulations. However, the complexation of $\text{UO}_2(\text{OH})_3^-$ with Ca^{2+} cations
22 has been distinctly identified in the surface density maps (as illustrated in Fig. 5(b)). As
23 expected, the PMF curve (Fig. 4) reveals that the sorption of $\text{UO}_2(\text{OH})_3^-$ complex is much

1 weaker but two distinct minima can be seen at the same distance from the Si-bridging
2 site as for the bare UO_2^{2+} ion with the energy barriers of about ~ 1.8 and ~ 0.3 kcal/mol,
3 respectively.

4



5

6 **Figure 4.** Adsorption free energy profiles of uranyl (left) and Na^+ (right) as functions of
7 their distance from the Si-bridging sorption site on C-S-H surface.

8

9 The adsorption free energy of UO_2^{2+} cation coordinated with gluconate has been
10 calculated next (solid yellow line in Fig. 4). The free energy of adsorption of the
11 UO_2^{2+} /gluconate complex is comparable to the one of the hydrolysed ion. However, a

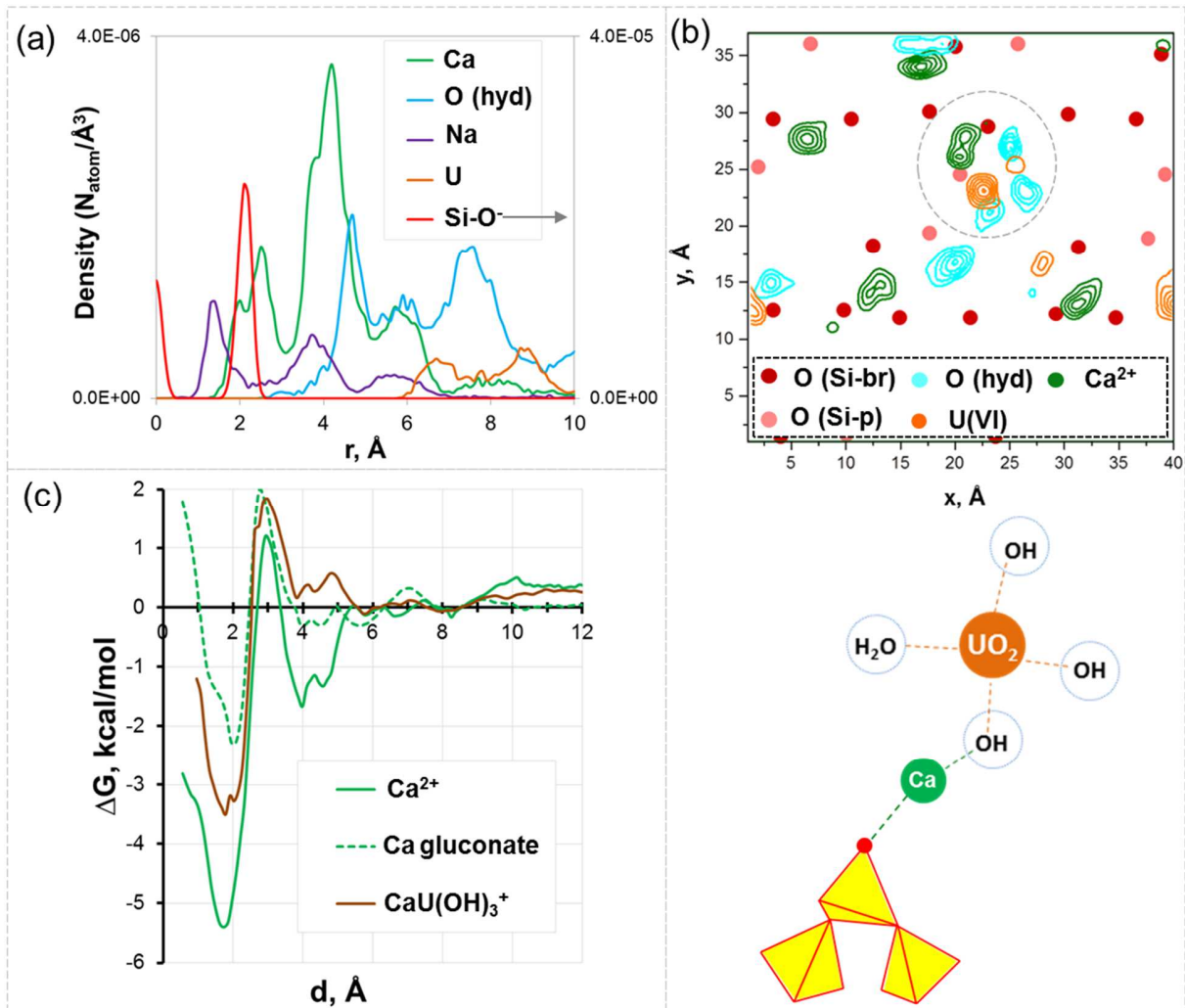
1 distinct difference in the binding energies can be observed: there is no clear separation
2 between outer- and inner-sphere complexation with a broad shallow energy minimum
3 found at distances $d > 4 \text{ \AA}$. It can be concluded that the presence of gluconate has a
4 much more important effect on the UO_2^{2+} surface sorption, compared to Ca^{2+} , and there
5 is more than a threefold decrease of the free energy minimum while pulling the position
6 of the minimum further away from the surface ($d \approx 4.5 \text{ \AA}$).

7 In combination with the results from the PMF calculations in bulk solution
8 ($\text{UO}_2(\text{OH})_3^-/\text{Ca}^{2+}$), it would therefore be presumed that the $\text{UO}_2(\text{OH})_3^-$ complex will
9 preferably form a stable association with Ca^{2+} cations bound to the surface. Similar
10 behaviour has been observed for uranyl complexation on Ca bentonite at high pH
11 conditions (Philipp et al., 2019), where inner-sphere adsorption was found despite an
12 anionic character of predominant aqueous species, and 4-fold coordination of U(VI)
13 surface complexes has been proven experimentally suggesting the possible mediating
14 contribution of Ca^{2+} cations.

15 Finally, the adsorption free energy of the identified $\text{CaUO}_2(\text{OH})_3^+$ complex
16 (Fig. 5(b)) has also been analyzed. In our model, the C-S-H surface does not have
17 homogeneous distribution of sorption sites of the same type, so the free energy profile
18 for an individual case will also slightly depend on the neighboring sites and sorbed
19 cations. Thus, the PMF curves for Ca^{2+} and Ca gluconate have been analyzed for the
20 same sorption site to provide a better reference for comparison. The main energy
21 minima that correspond to inner-sphere complexation with the deprotonated silanol
22 group can be found at about $\sim 2 \text{ \AA}$ (see Fig. 5 (c)). It can be clearly seen that the sorption
23 of $\text{CaUO}_2(\text{OH})_3^+$ is still weaker than for Ca^{2+} , but stronger than for Ca gluconate. Thus, it

1 can be assumed that $\text{CaUO}_2(\text{OH})_3^+$ will become an important competitor for the sorption
 2 sites in the presence of gluconate at the interface.

3



4

5 **Figure 5.** Atomic density profiles of solution species near the C-S-H surface (a), atomic
 6 density contour maps of time-averaged surface distributions of selected
 7 atoms at $d \approx 4-7$ \AA from the surface with the schematic representation of the
 8 surface ternary complex (b), and adsorption free energy profile of Ca
 9 complexes as functions of their distance from the Si-bridging sorption site (c).

1

2 It has previously been reported that U(VI) sorption is the strongest on C-S-H with
3 lower Ca/Si ratios in the absence of alkali (Tits et al., 2011). Our present work is
4 consistent with these results. We find that there are two main mechanisms controlling
5 the U(VI) sorption on the C-S-H surface: the binding to unoccupied deprotonated
6 silanols and the formation of ternary surface complex with Ca^{2+} cations. It has to be
7 mentioned that minor fraction ($< 5\%$) of other possible species ($\text{UO}_2(\text{OH})_2^0$, $\text{Ca}(\text{OH})^+$,
8 $\text{UO}_2(\text{OH})^+$, UO_2^{2+} , etc) will also contribute to surface sorption, even though they were not
9 analysed in detail in this work. For C-S-H with higher Ca/Si ratio and at higher pH, U(VI)
10 will mostly be found as a $\text{UO}_2(\text{OH})_4^{2-}$ complex and a larger fraction of Ca will be present
11 as $\text{Ca}(\text{OH})^+$. Therefore, it can be assumed that the direct binding to the surface oxygens
12 would be less probable, and the sorption through the formation of ternary complexes will
13 be reduced due to the less favourable binding with $\text{Ca}(\text{OH})^+$ compared to Ca^{2+} , as it was
14 discussed above. Several recent spectroscopic works (Tits et al., 2011; Macé et al.,
15 2013; Tits et al., 2015) have shown that three distinguishable types of U(VI) species can
16 be identified in the cementitious systems: (i) surface complexed; (ii) incorporated; (iii)
17 precipitated. The suggested incorporated U(VI) species should not be affected by the
18 presence of organics in the pore solution, so they were not considered in this study.

19 Additionally, we have analyzed the sorption of Na^+ cations on the Si-bridging site. It
20 has been previously confirmed that the nature of interaction between alkali and C-S-H is
21 electrostatic, and Na^+ will preferably sorb on the external surfaces of C-S-H particles
22 (Bach et al., 2013; Henocq, 2017). In our simulations, it was observed that Na^+ cations
23 are strongly attracted by the surface and most of them are found surface-bound for the

1 entire time of the equilibrium MD simulation run. Na^+ has an ionic radius similar to Ca^{2+} ,
2 but its solvation shell is weaker due to the lower charge and lower hydration energy.
3 Thus, much less energy is required to replace a water molecule in its first coordination
4 sphere by a negatively charged surface oxygen. It can be seen from the adsorption free
5 energy profile (Fig.4) that there is almost no energy barrier to overcome for Na^+ to sorb
6 on the Si-bridging surface site. Also, the sorption behaviour of Na^+ is very similar to that
7 of the Ca^{2+} /gluconate complex while the energy gain is almost twice as large
8 (~ -4.5 kcal/mol for the former vs ~ -2.5 for the latter). It can be concluded that Na^+
9 cations in solution can be very important competitors for the surface sorption sites, they
10 are able to replace Ca^{2+} and Ca^{2+} /gluconate complex on the C-S-H surface and affect
11 the $\text{UO}_2(\text{OH})_3^-$ adsorption. However, the peak position of Na^+ density at the distance of
12 $\sim 1\text{-}2$ Å from the Si-pairing silanols shows that Na^+ is able to sorb on the sites that are
13 less attractive for Ca^{2+} , most probably due to the difference in their charges (Fig. 5(a)).
14 Thus, the noticeable effect of Na^+ on the sorption properties of C-S-H will be more
15 pronounced at higher concentrations when the free sorption sites would be saturated.

16

17 **4. Conclusions**

18 The most probable mechanisms of molecular interactions in the ternary system
19 C-S-H / U(VI) / gluconate have been quantitatively analyzed and described using
20 classical and constrained molecular dynamics simulations. It is shown that complex
21 formation between uranyl hydroxides and Ca^{2+} cations at the C-S-H aqueous interfaces
22 has an important role in the overall sorption process. The existence of stable surface

1 ternary complexes of $\text{UO}_2(\text{OH})_3^-$ and Ca^{2+} were first identified using unconstrained MD
2 simulations, then their adsorption free energies characterizing specific surface sites
3 were quantitatively evaluated by the PMF calculations. Additionally, it was observed that
4 $\text{UO}_2(\text{OH})_3^-$ complex can bind directly to the unoccupied deprotonated surface silanols
5 increasing its total adsorption on C-S-H surfaces with low Ca/Si ratios, which agrees well
6 with available data in the literature.

7 The effect of gluconate ions on the U(VI) uptake by the C-S-H surfaces has been
8 found to be indirect. We have shown that gluconate forms stable complexes with Ca^{2+} ,
9 decreasing the strength of its binding to the surface sorption sites. As a result, it would
10 be easier for Ca-uranyl complexes to substitute Ca^{2+} , thus potentially increasing the
11 uptake of U(VI) by the C-S-H phases. Finally, Na^+ is proven to be an important
12 competitor for certain surface sorption sites and can potentially affect the equilibrium
13 properties of the interface. However, C-S-H surfaces provide numerous other sorption
14 sites for Na^+ ions, and the effect of the competitive alkali presence would be noticeable
15 once these available sorption sites are occupied.

16 The suggested mechanisms of U(VI) sorption on the C-S-H surface with low Ca/Si
17 ratios can be studied for other actinides that were proven to be stabilized by Ca^{2+} in
18 alkaline solutions. C-S-H phases with low Ca/Si ratio are the model for low pH cement
19 and degraded cements. Therefore, it is crucial to atomistically model cement at other
20 degradation stages for the most comprehensive description of the molecular
21 mechanisms involved in U(VI) uptake by cementitious materials. Further studies will
22 gauge the effect of gluconate on U(VI) sorption on C-S-H phases with higher Ca/Si ratio.

1

2 **Acknowledgements**

3 The study was supported by the industrial chair “Storage and Disposal of Radioactive
4 Waste” at the Institut Mines-Télécom Atlantique, funded by ANDRA, Orano, and EDF.
5 A.G.K. acknowledges additional support from the HSE University Basic Research
6 Program funded by the Russian Academic Excellence Project '5-100'. All calculations
7 were performed using the supercomputing resources at CCIPL (Centre de Calcul
8 Intensif des Pays de La Loire) and GENCI (Grand Équipement National de Calcul
9 Intensif; projects A0020906921, A0040906921, and A0060906921). Fruitful discussions
10 with Dr. C. Landesman (SUBATECH) and Dr. P. Henocq (ANDRA) are also gratefully
11 acknowledged.

1 **References**

- 2 Allen, M.P., Tildesley, D.J. (2017) *Computer Simulation of Liquids*. 2nd edition, *Oxford*
3 *University Press*, New York, 626pp.
- 4 Altmaier, M., Neck, V., Fanghänel, T., 2008. Solubility of Zr(IV), Th(IV) and Pu(IV)
5 hydrous oxides in CaCl₂ solutions and the formation of ternary Ca-M(IV)-OH
6 complexes. *Radiochim. Acta* 96 (9-11), pp. 541-550.
7 <https://doi.org/10.1524/ract.2008.1535>
- 8 Androniuk, I., Landesman, C., Henocq, P., Kalinichev, A.G., 2017. Adsorption of
9 gluconate and uranyl on C-S-H phases: Combination of wet chemistry experiments
10 and molecular dynamics simulations for the binary systems. *Phys. Chem. Earth*
11 *Parts ABC* 99, 194–203. <https://doi.org/10.1016/j.pce.2017.05.005>
- 12 Bach, T.T.H., Chabas, E., Pochard, I., Cau Dit Coumes, C., Haas, J., Frizon, F., Nonat,
13 A., 2013. Retention of alkali ions by hydrated low-pH cements: Mechanism and
14 Na⁺/K⁺ selectivity. *Cem. Concr. Res.* 51, 14–21.
15 <https://doi.org/10.1016/j.cemconres.2013.04.010>
- 16 Beaudoin, J.J., Raki, L., Alizadeh, R., 2009. A ²⁹Si MAS NMR study of modified C–S–H
17 nanostructures. *Cem. Concr. Compos.* 31, 585–590.
18 <https://doi.org/10.1016/j.cemconcomp.2008.11.004>
- 19 Birjkumar, K.H., Bryan, N.D., Kaltsoyannis, N., 2011. Computational investigation of the
20 speciation of uranyl gluconate complexes in aqueous solution. *Dalton Trans.* 40,
21 11248. <https://doi.org/10.1039/c1dt11086a>
- 22 Braun, E., Gilmer, J., Mayes, H.B., Mobley, D.L., Monroe, J.I., Prasad, S., Zuckerman,
23 D.M., 2019. Best Practices for Foundations in Molecular Simulations [Article v1.1].
24 *Living J. Comp. Mol. Sci.* 1(1), 5957. <https://doi.org/10.33011/livecoms.1.1.5957>
- 25 Chaudhari, O., Biernacki, J.J., Northrup, S., 2017. Effect of carboxylic and
26 hydroxycarboxylic acids on cement hydration: experimental and molecular modeling
27 study. *J. Mater. Sci.* 52, 13719–13735. <https://doi.org/10.1007/s10853-017-1464-0>
- 28 Chen, J.J., Thomas, J.J., Taylor, H.F.W., Jennings, H.M., 2004. Solubility and structure
29 of calcium silicate hydrate. *Cem. Concr. Res.* 34, 1499-1519.
30 <https://doi.org/10.1016/j.cemconres.2004.04.034>

1 Choppin, G.R., Mathur, J.N., 1991. Hydrolysis of actinyl(VI) cations. *Radiochim. Acta*
2 52–53, 25–28. <https://doi.org/10.1524/ract.1991.5253.1.25>

3 Churakov, S.V., Labbez, C., Pegado, L., Sulpizi, M., 2014. Intrinsic acidity of surface
4 sites in calcium silicate hydrates and its implication to their electrokinetic. properties.
5 *J. Phys. Chem. C* 118, 11752–11762. <https://doi.org/10.1021/jp502514a>

6 Clavaguéra-Sarrio, C., Hoyau, S., Ismail, N., Marsden, C.J., 2003. Modeling Complexes
7 of the Uranyl Ion $\text{UO}_2\text{L}_2^{n+}$: Binding Energies, Geometries, and Bonding Analysis.
8 *J. Phys. Chem. A* 107 (22), 4515–4525. <https://doi.org/10.1021/jp027243t>

9 Colàs, E., Grivé, M., Rojo, I., 2013. Complexation of uranium(VI) by gluconate in alkaline
10 solutions. *J. Solut. Chem.* 42, 1545–1557.
11 <https://doi.org/10.1007/s10953-013-0048-0>

12 Cong, X., Kirkpatrick, R.J., 1996. ^{29}Si MAS NMR study of the structure of calcium silicate
13 hydrate. *Adv. Cem. Based Mater.* 3, 144–156. [https://doi.org/10.1016/S1065-](https://doi.org/10.1016/S1065-7355(96)90046-2)
14 [7355\(96\)90046-2](https://doi.org/10.1016/S1065-7355(96)90046-2)

15 Cygan, R.T., Liang, J.-J., Kalinichev, A.G., 2004. Molecular models of hydroxide,
16 oxyhydroxide, and clay phases and the development of a general force field.
17 *J. Phys. Chem. B* 108, 1255–1266. <https://doi.org/10.1021/jp0363287>

18 Dong, W., Ball, W.P., Liu, C., Wang, Z., Stone, A.T., Bai, J., Zachara, J.M., 2005.
19 Influence of calcite and dissolved calcium on uranium(VI) sorption to a Hanford
20 subsurface sediment. *Environ. Sci. Technol.* 39, 7949–7955.
21 <https://doi.org/10.1021/es0505088>

22 Drobot, B., Bauer, A., Steudtner, R., Tsushima, S., Bok, F., Patzschke, M., Raff, J.,
23 Brendler, V., 2016. Speciation studies of metals in trace concentrations: The
24 mononuclear uranyl(VI) hydroxo complexes. *Analyt. Chem.* 88, 3548–3555.
25 <https://doi.org/10.1021/acs.analchem.5b03958>

26 Dufresne, A., Arayro, J., Zhou, T., Ioannidou, K., Ulm, F.-J., Pellenq, R., Béland, L.K.,
27 2018. Atomistic and mesoscale simulation of sodium and potassium adsorption in
28 cement paste. *J. Chem. Phys.* 149, 074705. <https://doi.org/10.1063/1.5042755>

29 Duvail, M., Dumas, T., Paquet, A., Coste, A., Berthon, L. Guilbaud, P., 2019. UO_2^{2+}
30 structure in solvent extraction phases resolved at molecular and supramolecular

1 scales: a combined molecular dynamics, EXAFS and SWAXS approach. *Phys.*
2 *Chem. Chem. Phys.* 21, 7894-7906. <https://doi.org/10.1039/C8CP07230B>

3 Fellhauer, D., Neck, V., Altmaier, M., Lützenkirchen, J., Fanghänel, T., 2010. Solubility
4 of tetravalent actinides in alkaline CaCl₂ solutions and formation of Ca₄[An(OH)₈]⁴⁺
5 complexes: A study of Np(IV) and Pu(IV) under reducing conditions and the
6 systematic trend in the An(IV) series. *Radiochim. Acta* 98, 541-548.
7 <https://doi.org/10.1524/ract.2010.1751>

8 Fellhauer, D., Altmaier, M., Gaona, X., Lützenkirchen, J., Fanghänel, T., 2016. Np(V)
9 solubility, speciation and solid phase formation in alkaline CaCl₂ solutions. Part II:
10 Thermodynamics and implications for source term estimations of nuclear waste
11 disposal. *Radiochim. Acta* 104 (6), 381-397. <https://doi.org/10.1515/ract-2015-2490>

12 Fox, P.M., Davis, J.A., Zachara, J.M., 2006. The effect of calcium on aqueous
13 uranium(VI) speciation and adsorption to ferrihydrite and quartz. *Geochim.*
14 *Cosmochim. Acta* 70, 1379–1387. <https://doi.org/10.1016/j.gca.2005.11.027>

15 Gaona, X., Kulik, D.A., Macé, N., Wieland, E., 2012. Aqueous–solid solution
16 thermodynamic model of U(VI) uptake in C–S–H phases. *Appl. Geochem.* 27, 81–
17 95. <https://doi.org/10.1016/j.apgeochem.2011.09.005>

18 García, D., Grivé, M., Duro, L., Brassinnes, S., de Pablo, J., 2018. The potential role of
19 the degradation products of cement superplasticizers on the mobility of
20 radionuclides. *Appl. Geochem.* 98, 1–9.
21 <https://doi.org/10.1016/j.apgeochem.2018.09.004>

22 García-Hernández, M., Willnauer, C., Krüger, S., Moskaleva, L.V., Rösch, N., 2006.
23 Systematic DFT study of gas phase and solvated uranyl and neptunyl complexes
24 [AnO₂X₄]ⁿ (An = U, Np; X = F, Cl, OH, n = -2; X = H₂O, n = +2). *Inorg. Chem.* 45,
25 1356–1366. <https://doi.org/10.1021/ic051492p>

26 Glasser, F.P., Marchand, J., Samson, E., 2008. Durability of concrete — Degradation
27 phenomena involving detrimental chemical reactions. *Cem. Concr. Res.* 38, 226–
28 246. <https://doi.org/10.1016/j.cemconres.2007.09.015>

29 Grambow, B., 2016. Geological disposal of radioactive waste in clay. *Elements* 12, 239-
30 245. <https://doi.org/10.2113/gselements.12.4.239>

1 Grangeon, S., Claret, F., Roosz, C., Sato, T., Gaboreau, S., Linard, Y., 2016. Structure
2 of nanocrystalline calcium silicate hydrates: insights from X-ray diffraction,
3 synchrotron X-ray absorption and nuclear magnetic resonance. *J. Appl. Crystallogr.*
4 49, 771–783. <https://doi.org/10.1107/S1600576716003885>

5 Grangeon, S., Fernandez-Martinez, A., Baronnet, A., Marty, N., Poulain, A., Elkaïm, E.,
6 Roosz, C., Gaboreau, S., Henocq, P., Claret, F., 2017. Quantitative X-ray pair
7 distribution function analysis of nanocrystalline calcium silicate hydrates: a
8 contribution to the understanding of cement chemistry. *J. Appl. Crystallogr.* 50, 14–
9 21. <https://doi.org/10.1107/S1600576716017404>

10 Greathouse, J. A., O'Brien, R. J., Bemis, G., Pabalan, R. T., 2002. Molecular Dynamics
11 Study of Aqueous Uranyl Interactions with Quartz (010). *J. Phys. Chem. B* 106 (7),
12 1646-1655. <https://doi.org/10.1021/jp013250q>

13 Grossfield, A., 2014. An Implementation of WHAM: the Weighted Histogram Analysis
14 Method Version 2.0.9.
15 <http://membrane.urmc.rochester.edu/sites/default/files/wham/doc.pdf>

16 Grossfield, A., Patrone, P.N., Roe, D.R., Schulz, A.J., Siderius, D.W., Zuckerman, D.M.,
17 2018, Best Practices for Quantification of Uncertainty and Sampling Quality in
18 Molecular Simulations [Article v1.0]. *Living J Comput Mol Sci.* 1(1), 5067.
19 <https://doi.org/10.33011/livecoms.1.1.5067>

20 Guilbaud, P., Wipff, G., 1996. Force field representation of the UO_2^{2+} cation from free
21 energy MD simulations in water. Tests on its 18-crown-6 and NO_3^- adducts, and on
22 its calix[6]arene⁶⁻ and CMPO complexes. *J. Mol. Struct.: THEOCHEM* 366, 55-63.
23 [https://doi.org/10.1016/0166-1280\(96\)04496-X](https://doi.org/10.1016/0166-1280(96)04496-X)

24 Hamid, S.A., 1981. The crystal structure of the 11 Å natural tobermorite
25 $\text{Ca}_{2.25}[\text{Si}_3\text{O}_{7.5}(\text{OH})_{1.5}] \cdot 1\text{H}_2\text{O}$. *Z. für Kristallogr.* 154, 189-198.

26 Harfouche, M., Wieland, E., Dähn, R., Fujita, T., Tits, J., Kunz, D., Tsukamoto, M., 2006.
27 EXAFS study of U(VI) uptake by calcium silicate hydrates. *J. Colloid Interface Sci.*
28 303, 195–204. <https://doi.org/10.1016/j.jcis.2006.07.019>

29 Häußler, V., Amayri, S., Beck, A., Platte, T., Stern, T.A., Vitova, T., Reich, T., 2018.
30 Uptake of actinides by calcium silicate hydrate (C-S-H) phases. *Appl. Geochem.*
31 <https://doi.org/10.1016/j.apgeochem.2018.08.021>

- 1 Henocq, P., 2017. A sorption model for alkalis in cement-based materials – Correlations
2 with solubility and electrokinetic properties. *Phys. Chem. Earth Parts ABC* 99, 184–
3 193. <https://doi.org/10.1016/j.pce.2017.05.004>
- 4 Hill, J., Harris, A.W., Manning, M., Chambers, A., Swanton, S.W., 2006. The effect of
5 sodium chloride on the dissolution of calcium silicate hydrate gels. *Waste Manag.*
6 26, 758–768. <https://doi.org/10.1016/j.wasman.2006.01.022>
- 7 Kalinichev, A.G., Wang, J., Kirkpatrick, R.J., 2007. Molecular dynamics modeling of the
8 structure, dynamics and energetics of mineral–water interfaces: Application to
9 cement materials. *Cem. Concr. Res.* 37, 337–347.
10 <https://doi.org/10.1016/j.cemconres.2006.07.004>
- 11 Kästner, J., 2011. Umbrella sampling. *Wiley Interdiscipl. Rev.: Comput. Mol. Sci.* 1, 932–
12 942. <https://doi.org/10.1002/wcms.66>
- 13 Keith-Roach, M.J., 2008. The speciation, stability, solubility and biodegradation of
14 organic co-contaminant radionuclide complexes: A review. *Sci. Total Environ.* 396,
15 1–11. <https://doi.org/10.1016/j.scitotenv.2008.02.030>
- 16 Kerisit, S., Liu, C., 2014. Molecular Dynamics Simulations of Uranyl and Uranyl
17 Carbonate Adsorption at Aluminosilicate Surfaces. *Environ. Sci. Technol.* 48 (7),
18 3899-3907. <https://doi.org/10.1021/es405387c>
- 19 Kirkpatrick, R.J., Kalinichev, A.G., Hou, X., Struble, L., 2005a. Experimental and
20 molecular dynamics modeling studies of interlayer swelling: water incorporation in
21 kanemite and ASR gel. *Mater. Struct.* 38, 449–458.
22 <https://doi.org/10.1007/BF02482141>
- 23 Kirkpatrick, R.J., Kalinichev, A.G., Wang, J., 2005b. Molecular dynamics modelling of
24 hydrated mineral interlayers and surfaces: structure and dynamics. *Mineral. Mag.*
25 69, 289–308. <https://doi.org/10.1180/0026461056930251>
- 26 Kořátková, J., Zatloukal, J., Reiterman, P., Kolář, K., 2017. Concrete and cement
27 composites used for radioactive waste deposition. *J. Env. Rad.* 178-179, 147-155.
28 <https://doi.org/10.1016/j.jenvrad.2017.08.012>
- 29 Krestou, A., Panias, D., 2004. Uranium (VI) speciation diagrams in the $\text{UO}_2^{2+}/\text{CO}_3^{2-}/\text{H}_2\text{O}$
30 system at 25°C. *Eur. J. Miner. Process. Environ. Prot.* 4, 113–129.

- 1 Kumar, A., Walder, B.J., Kunhi Mohamed, A., Hofstetter, A., Srinivasan, B., Rossini,
2 A.J., Scrivener, K., Emsley, L., Bowen, P., 2017. The atomic-level structure of
3 cementitious calcium silicate hydrate. *J. Phys. Chem. C* 121, 17188–17196.
4 <https://doi.org/10.1021/acs.jpcc.7b02439>
- 5 Kunhi Mohamed, A., Parker, S.C., Bowen, P., Galmarini, S., 2018. An atomistic building
6 block description of C-S-H - Towards a realistic C-S-H model. *Cem. Concr. Res.*
7 107, 221–235. <https://doi.org/10.1016/j.cemconres.2018.01.007>
- 8 Labbez, C., Pochard, I., Jönsson, B., Nonat, A., 2011. C-S-H/solution interface:
9 Experimental and Monte Carlo studies. *Cem. Concr. Res.* 41, 161–168.
10 <https://doi.org/10.1016/j.cemconres.2010.10.002>
- 11 Loganathan, N., Kalinichev, A.G., 2017. Quantifying the mechanisms of site-specific ion
12 exchange at an inhomogeneously charged surface: Case of Cs⁺ /K⁺ on hydrated
13 muscovite mica. *J. Phys. Chem. C* 121, 7829–7836.
14 <https://doi.org/10.1021/acs.jpcc.6b13108>
- 15 Lothenbach, B., Nonat, A., 2015. Calcium silicate hydrates: Solid and liquid phase
16 composition. *Cem. Conc. Res.* 78, 57-70.
17 <http://dx.doi.org/10.1016/j.cemconres.2015.03.019>
- 18 Macé, N., Wieland, E., Dähn, R., Tits, J., Scheinost, A.C., 2013. EXAFS investigation on
19 U(VI) immobilization in hardened cement paste: influence of experimental conditions
20 on speciation. *Radiochim. Acta* 101, 379–389.
21 <https://doi.org/10.1524/ract.2013.2024>
- 22 Merlino, S., Bonaccorsi, E., Armbruster, T., 2001. The real structure of tobermorite 11
23 angstrom: normal and anomalous forms, OD character and polytypic modifications.
24 *Eur. J. Mineral.* 13(3), 577-590. <https://doi.org/10.1127/0935-1221/2001/0013-0577>
- 25 Mishra, R. K., Mohamed, A. K., Geissbühler, D., Manzano, H., Jamil, T., Shahsavari, R.,
26 Kalinichev, A. G., Galmarini, S., Tao, L., Heinz, H., Pellenq, R., van Duin, A. C. T.,
27 Parker, S. C., Flatt, R. J., and Bowen, P., 2017. CEMFF: A force field database for
28 cementitious materials including validations, applications and opportunities. *Cem.*
29 *Concr. Res.* 102, 68-89. <https://doi.org/10.1016/j.cemconres.2017.09.003>

- 1 Moll, H., Rossberg, A., Steudtner, R., Drobot, B., Müller, K., Tsushima, S., 2014.
2 Uranium(VI) chemistry in strong alkaline solution: speciation and oxygen exchange
3 mechanism. *Inorg. Chem.* 53, 1585–1593. <https://doi.org/10.1021/ic402664n>
- 4 Mutisya, S. M., de Almeida, J. M., and Miranda, C. R., 2017. Molecular simulations of
5 cement based materials: A comparison between first principles and classical force
6 field calculations. *Comput. Mater. Sci.* 138, 392-402.
7 <https://doi.org/10.1016/j.commatsci.2017.07.009>
- 8 Nalet, C., Nonat, A., 2016. Effects of functionality and stereochemistry of small organic
9 molecules on the hydration of tricalcium silicate. *Cem. Concr. Res.* 87, 97-104.
10 <https://doi.org/10.1016/j.cemconres.2016.06.002>
- 11 Newcomb, K., Tiwari, S.P., Rai, N., Maginn, E.J., 2018. A molecular dynamics
12 investigation of actinyl–ligand speciation in aqueous solution. *Phys. Chem. Chem.*
13 *Phys.* 20, 15753-15763. <https://doi.org/10.1039/C8CP01944D>.
- 14 Orozco, C.A., Chun, B.W., Geng, G., Emwas, A.H., Monteiro, P.J.M., 2017.
15 Characterization of the bonds developed between calcium silicate hydrate and
16 polycarboxylate-based superplasticizers with silyl functionalities. *Langmuir* 33,
17 3404–3412. <https://doi.org/10.1021/acs.langmuir.6b04368>
- 18 Pellenq, R.J.-M., Kushima, A., Shahsavari, R., Van Vliet, K.J., Buehler, M.J., Yip, S.,
19 Ulm, F.-J., 2009. A realistic molecular model of cement hydrates. *Proc. Natl. Acad.*
20 *Sci.* 106, 16102–16107. <https://doi.org/10.1073/pnas.0902180106>
- 21 Philipp, T., Aldin Azzam, S.S., Rossberg, A., Huittinen, N., Schmeide, K., Stumpf, T.,
22 2019. U(VI) sorption on Ca-bentonite at (hyper)alkaline conditions – Spectroscopic
23 investigations of retention mechanisms. *Sci. Total Environ.* 676, 469–481.
24 <https://doi.org/10.1016/j.scitotenv.2019.04.274>
- 25 Plimpton, S., 1995. Fast parallel algorithms for short-range molecular dynamics.
26 *J. Comput. Phys.* 117, 1–19. <https://doi.org/10.1006/jcph.1995.1039>
- 27 Pointeau, I., Landesman, C., Giffaut, E., Reiller, P., 2004. Reproducibility of the uptake
28 of U(VI) onto degraded cement pastes and calcium silicate hydrate phases.
29 *Radiochim. Acta* 92, 645–650. <https://doi.org/10.1524/ract.92.9.645.55008>.

- 1 Pointeau, I., Hainos, D., Coreau, N., Reiller, P., 2006. Effect of organics on selenite
2 uptake by cementitious materials. *Waste Manag.* 26, 733–740.
3 <https://doi.org/10.1016/j.wasman.2006.01.026>
- 4 Pointeau, I., Coreau, N., Reiller, P.E., 2008. Uptake of anionic radionuclides onto
5 degraded cement pastes and competing effect of organic ligands. *Radiochim. Acta*
6 96, 367-374. <https://doi.org/10.1524/ract.2008.1503>
- 7 Rabung, T., Altmaier, M., Neck, V., Fanghänel, T., 2008. A TRLFS study of Cm(III)
8 hydroxide complexes in alkaline CaCl₂ solutions. *Radiochim. Acta* 96, 551-559.
9 <https://doi.org/10.1524/ract.2008.1536>
- 10 Richardson, I.G., Skibsted, J., Black, L., Kirkpatrick, R.J., 2010. Characterisation of
11 cement hydrate phases by TEM, NMR and Raman spectroscopy. *Adv. Cem. Res.*
12 22, 233–248. <https://doi.org/10.1680/adcr.2010.22.4.233>
- 13 Richter, C., Müller, K., Drobot, B., Steudtner, R., Großmann, K., Stockmann, M.,
14 Brendler, V., 2016. Macroscopic and spectroscopic characterization of uranium(VI)
15 sorption onto orthoclase and muscovite and the influence of competing Ca²⁺.
16 *Geochim. Cosmochim. Acta* 189, 143–157.
17 <https://doi.org/10.1016/j.gca.2016.05.045>
- 18 Roosz, C., Vieillard, P., Blanc, P., Gaboreau, S., Gailhanou, H., Braithwaite, D.,
19 Montouillout, V., Denoyel, R., Henocq, P., Madé, B., 2018. Thermodynamic
20 properties of C-S-H, C-A-S-H and M-S-H phases: Results from direct measurements
21 and predictive modelling. *Appl. Geochem.* 92, 140–156.
22 <https://doi.org/10.1016/j.apgeochem.2018.03.004>
- 23 Saleh, A.Sh., Lee, J.-Y., Jo, Y., Yun, J.-I., 2018. Uranium(VI) sorption complexes on
24 silica in the presence of calcium and carbonate. *J. Environ. Radioact.* 182, 63–69.
25 <https://doi.org/10.1016/j.jenvrad.2017.11.006>
- 26 Smith, K.F., Bryan, N.D., Swinburne, A.N., Bots, P., Shaw, S., Natrajan, L.S.,
27 Mosselmans, J.F.W., Livens, F.R., Morris, K., 2015. U(VI) behaviour in hyperalkaline
28 calcite systems. *Geochim. Cosmochim. Acta* 148, 343–359.
29 <https://doi.org/10.1016/j.gca.2014.09.043>

- 1 Stewart, B.D., Mayes, M.A., Fendorf, S., 2010. Impact of uranyl–calcium–carbonato
2 complexes on uranium(VI) adsorption to synthetic and natural sediments. *Environ.*
3 *Sci. Technol.* 44, 928–934. <https://doi.org/10.1021/es902194x>
- 4 Sugiyama, D., 2008. Chemical alteration of calcium silicate hydrate (C–S–H) in sodium
5 chloride solution. *Cem. Concr. Res.* 38, 1270–1275.
6 <https://doi.org/10.1016/j.cemconres.2008.06.002>
- 7 Szczerba, M., Kalinichev, A.G., 2016. Intercalation of ethylene glycol in smectites:
8 Several molecular simulation models verified by X-ray diffraction data. *Clays Clay*
9 *Miner.* 64, 488–502. <https://doi.org/10.1346/CCMN.2016.0640411>
- 10 Taylor, H.F.W., 1997. Cement Chemistry, Second Edition. Thomas Telford, 459 p.
- 11 Teich-McGoldrick, S.L., Greathouse, J.A., Cygan, R.T., 2014. Molecular dynamics
12 simulations of uranyl adsorption and structure on the basal surface of muscovite.
13 *Mol. Simul.* 40, 610–617. <https://doi.org/10.1080/08927022.2013.838675>
- 14 Tits, J., Geipel, G., Macé, N., Eilzer, M., Wieland, E., 2011. Determination of uranium(VI)
15 sorbed species in calcium silicate hydrate phases: A laser-induced luminescence
16 spectroscopy and batch sorption study. *J. Colloid Interface Sci.* 359, 248–256.
17 <https://doi.org/10.1016/j.jcis.2011.03.046>
- 18 Tits, J., Walther, C., Stumpf, T., Macé, N., Wieland, E., 2015. A luminescence line-
19 narrowing spectroscopic study of the uranium(VI) interaction with cementitious
20 materials and titanium dioxide. *Dalton Trans* 44 (3): 966-76.
21 <https://doi.org/10.1039/c4dt02172j>.
- 22 Tits, J., Wieland, E., 2018. Actinide sorption by cementitious materials (PSI Bericht
23 No. 18-02). Paul Scherrer Institut (PSI).
- 24 Viallis-Terrisse, H., Nonat, A., Petit, J.-C., 2001. Zeta-potential study of calcium silicate
25 hydrates interacting with alkaline cations. *J. Colloid Interface Sci.* 244, 58–65.
26 <https://doi.org/10.1006/jcis.2001.7897>
- 27 Wang, J., Wolf, R.M., Caldwell, J.W., Kollman, P.A., Case, D.A., 2004. Development
28 and testing of a general AMBER force field. *J. Comput. Chem.* 25, 1157–1174.
29 <https://doi.org/10.1002/jcc.20035>

1 Yu, P., Kirkpatrick, R.J., Poe, B., McMillan, P.F., Cong, X.D., 1999. Structure of calcium
2 silicate hydrate (C-S-H): Near-, mid-, and far-infrared spectroscopy. *J. Am. Ceram.*
3 *Soc.* 82, 742-748. <https://doi.org/10.1111/j.1151-2916.1999.tb01826.x>